

## ROSAT OBSERVATIONS OF X-RAY EMISSION FROM PLANETARY NEBULAE

MARTÍN A. GUERRERO, YOU-HUA CHU, AND ROBERT A. GRUENDL

Department of Astronomy, University of Illinois at Urbana-Champaign,  
1002 West Green Street, Urbana, IL 61801

E-mail: mar@astro.uiuc.edu, chu@astro.uiuc.edu, gruendl@astro.uiuc.edu

*Received 1999 December 23; accepted 2000 January*

## ABSTRACT

We have searched the entire ROSAT archive for useful observations to study X-ray emission from Galactic planetary nebulae (PNs). The search yields a sample of 63 PNs, which we call the ROSAT PN sample. About 20–25% of this sample show X-ray emission; these include 13 definite detections and three possible detections (at a  $2\sigma$  level). All X-ray sources in these PNs are concentrated near the central stars. Only A 30, BD+30°3639, and NGC 6543 are marginally resolved by the ROSAT instruments.

Three types of X-ray spectra are seen in PNs. Type 1 consists of only soft X-ray emission ( $<0.5$  keV), peaks at 0.1–0.2 keV, and can be fitted by blackbody models at temperatures  $1-2 \times 10^5$  K. Type 2 consists of harder X-ray emission, peaks at  $>0.5$  keV, and can be fitted by thin plasma emission models at temperatures of a few  $10^6$  K. Type 3 is a composite of a bright Type 1 component and a fainter Type 2 component.

Unresolved soft sources with Type 1 spectra or the soft component of Type 3 spectra are most likely photospheric emission from the hot central stars. Absorption cross sections are large for these soft-energy photons; therefore, only large, tenuous, evolved PNs with hot central stars and small absorption column densities have been detected.

The origin of hard X-ray emission from PNs is uncertain. PNs with Type 2 spectra are small, dense, young nebulae with relatively cool ( $\ll 10^5$  K) central stars, while PNs with Type 3 X-ray spectra are large, tenuous, evolved nebulae with hot central stars. The hard X-ray luminosities are also different between these two types of PNs, indicating perhaps different origins of their hard X-ray emission. Future Chandra and XMM observations with high spatial and spectral resolution will help to understand the origin of hard X-ray emission from PNs.

*Subject headings:* planetary nebulae: general – stars: AGB and post-AGB – X-rays: stars

## 1. INTRODUCTION

Planetary nebulae (PNs) are expected to emit weakly at X-ray wavelengths. X-ray emission from a PN was not detected until the mid 1980's, when de Korte et al. (1985) reported EXOSAT observations of NGC 1360. Soon afterward, data from the Einstein archive were used to discover X-ray emission from NGC 246, NGC 6853, NGC 7293, and A 33 (Tarafdar & Apparao 1988). Similarly, data from the EXOSAT archive were used to show X-ray emission from four more PNs, NGC 1535, NGC 4361, NGC 3587, and A 36 (Apparao & Tarafdar 1989). More recently, ROSAT observations have yielded additional detections: A 12, BD+30°3639, LoTr 5, and NGC 6543 (Kreysing et al. 1992); K 1-27 (Rauch, Koepen, & Werner 1994); K 1-16 (Hoare et al. 1995); and A 30 (Chu & Ho 1995). To date, a total of 16 PNs have been reported to emit X-rays.

All of the detections made prior to the ROSAT era were interpreted as soft X-ray emission from the hot (100,000–200,000 K) central star. In the more recent

ROSAT observations, *diffuse* X-ray emission from PNs has been reported (Kreysing et al. 1992 – A 12, LoTr 5, NGC 4361, NGC 6543 and NGC 6853; Chu & Ho 1995 – A 30; Leahy, Kwok, & Yin 1998 – BD+30°3639). This diffuse X-ray emission, if confirmed, is likely to originate from shock-heated gas.

ROSAT has provided both high spatial resolution to study the distribution of X-ray emission and high sensitivity to enable the spectral analysis of X-ray emission from PNs. Conway & Chu (1997) noted that X-ray emission of PNs can be divided into three different spectral types: (1) spectra with only soft ( $<0.4$  keV) X-ray emission, for example, NGC 6853 (Kreysing et al. 1992), NGC 246, NGC 1360, and K 1-16 (Hoare et al. 1995); (2) spectra that peak at greater than 0.5 keV, for example, BD+30°3639 (Arnaud, Borkowski, & Harrington 1996) and NGC 6543 (Kreysing et al. 1992); (3) spectra with both soft and hard components, for example, NGC 7293 (Leahy, Zhang, & Kwok 1994).

Despite the apparent success detecting X-ray emission

from PNs, some misidentifications and erroneous analyses have appeared in the literature. The misidentifications include A 12, A 33, and NGC 1535, as pointed out by Hoare et al. (1995), Conway & Chu (1997), and Chu, Gruendl, & Conway (1998), respectively. A detailed comparison between the X-ray and optical images reveals that the X-ray sources are located outside the optical boundary of these PNs. The diffuse-nature of the X-ray emission reported in LoTr 5, NGC 4361, and NGC 6853 has been disputed. The apparently extended morphology of LoTr 5 and NGC 4361 (Kreysing et al. 1992) are probably caused by the low signal-to-noise ratio available in the ROSAT All Sky Survey data, as a deep pointed ROSAT observation of LoTr 5 shows an unresolved source (Chu & Ho 1995), and an EUVE observation of NGC 4361 detects only a point source (Fruscione et al. 1995). The apparently extended morphology in NGC 6853 is caused by an electronic ghost image for photon energies below 0.2 keV (Chu, Kwitter, & Kaler 1993).

ROSAT observations of PNs have discovered  $\sim 50\%$  of the currently known X-ray sources in PNs. Furthermore, ROSAT has provided, for the first time, spatial and spectral information of X-ray emission from PNs. The large volume of ROSAT observations offers an excellent opportunity for archival studies. We have searched the ROSAT archive for observations that contain PNs within the central, unvignetted field of view. We find useful ROSAT observations for 80 PNs. Some of the observations were pointed at the PNs in question, while others were serendipitous observations pointed at objects projected near a PN. Only a small fraction of these observations of PNs have been analyzed and reported previously.

The ROSAT archive allows us to assemble the most complete set of X-ray observations of PNs possible. We have analyzed these observations to determine the spatial and spectral properties of X-ray emission for the PNs detected and the  $3\sigma$  upper limits for the non-detections. We have examined how absorption affects the detectability of hard and soft X-ray sources in PNs. We have further correlated the observed X-ray properties with extinction, distance, stellar and nebular properties, in order to interpret the X-ray observations of PNs. The results not only help us understand the origin of X-ray emission from PNs, but also provide a roadmap for future observations of PNs using the up-coming X-ray missions, e.g., Chandra Advanced X-ray Astrophysics Facility and X-ray Multi-mirror Mission.

This paper reports our work on ROSAT observations of PNs. In Section 2 we describe the PN sample and present our analyses and results. Section 3 discusses the detectability of X-ray emission from PNs, absorption effects

on the survey results, correlation between X-ray spectra and physical properties of the PNs, and physical nature of X-ray emission from PNs. A summary is given in Section 4.

## 2. X-RAY SURVEY OF PLANETARY NEBULAE IN THE ROSAT ARCHIVE

### 2.1. ROSAT Observations of Planetary Nebulae

ROSAT (RÖentgen SATellite) had two types of X-ray detectors onboard: the Position Sensitive Proportional Counter (PSPC) and the High Resolution Imager (HRI). The PSPC is sensitive to X-rays in the energy range of 0.1–2.4 keV. Its on-axis point spread function (PSF) has a FWHM  $\sim 25''$  and its spectral resolution is  $\sim 45\%$  at 1 keV. The spectral resolution below 0.28 keV can be augmented if observations are made both with and without a boron filter, as the boron filter blocks X-rays between 0.188 and 0.28 keV. The PSPC field of view is  $\sim 1^\circ$  in radius, but the PSF deteriorates rapidly and vignetting becomes significant beyond  $20'$  from the center (ROSAT Mission Description 1991). The HRI is sensitive to X-rays in the energy range of 0.1–2.0 keV, but has negligible spectral resolution. It has an in-flight, on-axis PSF of FWHM  $\sim 6''$  and a field of view of  $38' \times 38'$  (David et al. 1996). The soft X-ray response of these detectors makes ROSAT observations invaluable to study X-ray emission from PNs. ROSAT archival data can be obtained from the anonymous ftp site [legacy.gsfc.nasa.gov](http://legacy.gsfc.nasa.gov), or downloaded from the web site <http://heasarc.gsfc.nasa.gov/W3Browse>. Both of these sites are supported by the High Energy Astrophysics Science Archive Research Center (HEASARC) of Goddard Space Flight Center, NASA.

To search for useful ROSAT observations of PNs, we used the list of Galactic PNs in the “Strasbourg-ESO Catalogue of Galactic Planetary Nebulae” (Acker et al. 1992) at <ftp://cdsarc.u-strasbg.fr/cats/V/84>, and correlated the PN coordinates with the pointings of all archival ROSAT observations. In order to assure the highest quality for the data, we only selected those ROSAT observations with exposure times longer than 1,000 s. For the PSPC observations, we further restricted the selection to those in which the angular distances of the PNs to the field centers were less than  $20'$ . Eighty PNs<sup>1</sup> have ROSAT observations that meet these criteria. Of these, 55 have only PSPC observations, 8 have only HRI observations, and 17 have both PSPC and HRI observations.

Table 1 lists the 80 PNs and their ROSAT observations. Columns 1 and 2 give the galactic coordinates and names of PNs. Column 3 gives the ROSAT observation sequence number: “rp” stands for PSPC observations without any filter, “rf” for PSPC observations with the boron filter,

<sup>1</sup>M 1-67 is in the Acker et al.’s (1992) list of PNs and has ROSAT HRI observations, but we do not include it because it has been shown to be a ring nebula around a Pop. I Wolf-Rayet star (Crawford & Barlow 1991). Similarly, we exclude EGB 4 because it is likely produced by the strong wind from BZ Cam (Hollis et al. 1992), a white-dwarf star in a cataclysmic binary system (Kraft, Krzeminski, & Mumford 1969).

and “rh” for HRI observations. Columns 4 and 5 give the exposure time and the offset of the PN position from the pointing center. When two or more observations with the same instrument are available for a nebula, these observations have been aligned and merged into one file to increase the exposure time and to improve the signal-to-noise ratio. The merged files are used in our analysis.

Of these 80 nebulae, some are projected within or near a bright X-ray source and the identification of the PN emission is uncertain. Such is the case for: Ps 1, the PN in the globular cluster M 15; H 4-1, in the direction of the Virgo Cluster; H 2-12, Pe 2-8, and Wray 16-20, located in the direction of supernova remnants; and A 12, H 1-43, He 2-51, and M 1-30, too close to bright X-ray point sources. Therefore, we have excluded these objects from our final sample.

The final sample consists of 63 objects with PSPC observations (13 have additional HRI observations), and 8 objects with only HRI observations. Given the limited spectral information and sensitivity of the HRI observations, we will focus the statistical study on the sample of 63 PNs with PSPC observations. Hereafter, we will refer to this as the ROSAT PN sample.

## 2.2. X-ray Emission from Planetary Nebulae

To search for X-ray emission from PNs in the ROSAT sample, we have compared the PSPC X-ray images with the optical images extracted from the Digitized Sky Survey<sup>2</sup> (DSS). For each PN, we plot the X-ray contours over the optical image to determine whether X-ray emission is detected within the optical boundary of the nebula. We then define a source region that encompasses the entire nebula, use a surrounding annulus as a background region, prorate the background and compute the background-subtracted PSPC counts within the source region. For unresolved PNs, we use source regions that match the PSPC’s point spread function.

X-ray emission was detected in 13 PNs, of which NGC 7009 is the only detection not previously reported in the literature. Their identifications and X-ray counts are listed in Table 2. Columns 1 and 2 give their Galactic coordinates and names, column 3 the net PSPC counts detected within the nebulae, and column 4 the PSPC count rates. In order to facilitate comparisons with the non-detections, we have also listed the  $3\sigma$  values of the count rates in column 5. The X-ray spectral type (described below in this section) is given in column 6. Additional notes for some individual nebulae are given in Appendix A.

Table 2 contains all PNs confirmed to emit X-rays, with the exception of NGC 4361, which does not have pointed

ROSAT observations. We note that X-ray emission is also tentatively detected in three additional PNs at a  $2\sigma$  level. These three PNs are listed in Table 3, in which information similar to that in Table 2 is given. Follow-up observations are needed to confirm or reject the X-ray emission from these three PNs. For the remaining 47 PNs that are not detected by ROSAT observations, we have determined their  $3\sigma$  detection limits and listed them in Table 4.

Figure 1 shows the distributions of exposure time and the  $3\sigma$  detection limit of PSPC observations of the ROSAT PN sample. About 60% of the detections were made in observations with  $\leq 10$  ks exposure time. Many nondetections have very stringent  $3\sigma$  upper limits. Thus, it may be concluded that the data quality is high and that the non-detections are caused by low X-ray fluxes from these PNs instead of short exposure times.

To illustrate the distribution of X-ray emission within the PNs, Figure 2 displays X-ray images extracted from the PSPC observations alongside the DSS images extracted over the same field of view and overlaid by the X-ray contours. Figure 2 also shows two examples of PN misidentifications (A 12 and A 33). It can be seen that all 13 detected PNs have X-ray emission concentrated at the center of the nebula. None of the 13 X-ray sources in PNs are “clearly” resolved. Only after painstakingly analyses can one find that A 30 and BD+30°3639 are marginally resolved by the HRI (Chu, Chang, & Conway 1997; Leahy et al. 1998) and NGC 6543 marginally resolved by the PSPC (Kreysing et al. 1992). (By “marginally resolved” we mean that the FWHM of the surface brightness profile is not larger than 1.5 times the instrumental FWHM.)

We have extracted X-ray spectra of these 13 PNs from their PSPC observations. The corresponding PSPC count rate plots are displayed in Figure 3. These spectra can be roughly classified into three types, as noted by Conway & Chu (1997):

- Type 1 spectra have PSPC counts peaking near 0.1–0.2 keV and vanishing above 0.5 keV; this group includes NGC 246, NGC 1360, NGC 3587, NGC 6853, A 30, and K 1-16.
- Type 2 spectra have PSPC counts peaking at  $>0.5$  keV; this group includes NGC 6543 and BD+30°3639.
- Type 3 spectra have PSPC counts peaking strongly near 0.1–0.2 keV and weakly at 0.5–1.0 keV; this group includes NGC 7293 and LoTr 5.

The spectra of NGC 7009, A 36 and K 1-27, shown in Figure 4, are too noisy to be classified definitively. As their

<sup>2</sup>The Digitized Sky Survey is based on photographic data obtained using the UK Schmidt Telescope and the Oschin Schmidt Telescope on Palomar Mountain. The UK Schmidt was operated by the Royal Observatory of Edinburgh, with funding from the UK Science and Engineering Research Council, until 1988 June, and thereafter by the Anglo-Australian Observatory. The Palomar Observatory Sky Survey was funded by the National Geographic Society. The Oschin Schmidt Telescope is operated by the California Institute of Technology and Palomar Observatory. The plates were processed into the present compressed digital form with the permission of these institutes. The Digitized Sky Survey was produced at the Space Telescope Science Institute under US government grant NAGW-2166.

detected photons have energies mostly above 0.5 keV and do not peak at 0.1–0.2 keV, it is most likely that these three spectra are of Type 2.

The three types of spectra can be fitted by different models. Type 1 spectra can be fitted by blackbody models at temperatures of 100,000 to 200,000 K or atmospheric models of similar stellar effective temperatures (Chu et al. 1993; Hoare et al. 1995). Type 2 spectra can be fitted by thin plasma emission models (e.g., Raymond & Smith 1977) for a plasma temperature of a few  $10^6$  K (Arnaud et al. 1996). Type 3 spectra can be fitted by the combination of a blackbody model and a thin plasma emission model (Leahy et al. 1994).

### 3. DISCUSSION

#### 3.1. Detectability of X-ray Emission from Planetary Nebulae

In the ROSAT PN sample,  $\sim 20\%$  of the PNs are detected; their PSPC count rates range from 0.002 to 0.4 counts  $s^{-1}$ . The detection rate rises to  $\sim 25\%$ , if the tentative detections for NGC 2371-72, NGC 2392, and NGC 6572 are included. A similar detection rate, 25%, can be derived from the Einstein and EXOSAT observations of PNs (Tarafdar & Apparao 1988; Apparao & Tarafdar 1989) if misidentifications are disregarded.

Note that the aforementioned detection rate should not be interpreted as the fraction of PNs that emit X-rays, because the detectability depends on different factors. These include not only the X-ray luminosity and distance of the PN, but also a complex interplay among the X-ray spectrum of the PN, the intervening absorption, and the energy-dependent response of the detector. In the ROSAT energy band, the interstellar absorption cross section is large, in particular at the low energy end. Because the absorption is energy dependent, its effects on X-ray sources with different intrinsic spectra can be drastically different. To illustrate this, we have calculated the ratio of the absorbed and unabsorbed flux in the ROSAT PSPC band as a function of absorption column density,  $N_{\text{H}}$ , for two models of X-ray emission: a blackbody model for stellar photospheric emission, and the Raymond & Smith (1977) model for thin plasma emission. These two models are used because the blackbody model simulates a Type 1 spectrum and the thin plasma emission model simulates a Type 2 spectrum. Morrison & McCammon's (1983) effective cross section per hydrogen atom is used for the absorption, and solar abundances are used for the thin plasma emission.

Figure 5 shows the absorbed to unabsorbed flux ratios for blackbody emission at three temperatures appropriate for hot central stars of PNs (left panel) and for thin plasma emission at three plasma temperatures within  $1-4 \times 10^6$  K (right panel). The X-ray emission for a blackbody at  $1-2 \times 10^5$  K is very soft and the interstellar absorption cross section is very high in this soft band; therefore,

the blackbody emission is much more strongly absorbed by even a moderate column of intervening material than emission from a hot thin plasma.

To examine the range of absorption column densities commonly seen for PNs, we convert the optically determined extinction to an HI column density,  $N_{\text{HI}}$ , and use it to approximate the absorption column density,  $N_{\text{H}}$ . It should be born in mind that the absorption column density,  $N_{\text{H}}$ , consists of not only the atomic gas but also ionized gas and molecular gas, and therefore  $N_{\text{HI}}$  provides only a lower limit for  $N_{\text{H}}$ . A large number of PNs have  $c_{\text{H}\beta}$ , the logarithmic extinction at  $\text{H}\beta$ , available in the literature (e.g., Cahn, Kaler, & Stanghellini 1992; Tylenda et al. 1992). The extinction at  $\text{H}\beta$  can be related to the visual extinction  $A_{\text{v}}$  and to the color excess  $E(B-V)$  by  $A_{\text{v}} = 3.1 E(B-V) = 2.17 c_{\text{H}\beta}$ . Using Bohlin, Savage, & Drake's (1978) gas to dust ratio,  $N_{\text{HI}}/E(B-V) = 5.8 \times 10^{21} \text{ cm}^{-2} \text{ mag}^{-1}$ , we derive  $N_{\text{HI}}$  from  $c_{\text{H}\beta}$ .

Typical  $c_{\text{H}\beta}$  values of Galactic PNs range from a few tenths to greater than one, corresponding to  $A_{\text{v}}$  of 1–2 mag or  $N_{\text{HI}} = 2-4 \times 10^{21} \text{ cm}^{-2}$ . Figure 5 illustrates that blackbody emission would have been attenuated by factors of  $10^5$  to  $10^{10}$ , while emission from a thin plasma at  $2 \times 10^6$  K is attenuated by factors of a few tens. It is conceivable that the detectability of stellar photospheric emission is more heavily dependent on the intervening absorption and that most PNs' photospheric emission are attenuated below detection limit.

#### 3.2. Absorption Effects in the Survey Results

In order to examine the absorption effects in the X-ray observations of the ROSAT PN sample, we have listed the distance ( $d$ ), visual extinction ( $A_{\text{v}}$ ), and the corresponding HI column density ( $N_{\text{HI}}$ ) in Table 5. Histograms of the distribution of PNs with respect to  $A_{\text{v}}$ , distance, and Galactic latitude and longitude are presented in Figure 6.

It is clear from Figure 6 that the intervening absorption column severely limits the detection of X-ray emission from PNs: none in the ROSAT PN sample are detected with  $A_{\text{v}}$  greater than 1 mag. Indeed, most of the detections have  $A_{\text{v}} \leq 0.4$  mag. The only object detected with a high extinction,  $A_{\text{v}} = 1$  mag, is BD+30°3639, which has a Type 2 spectrum and is best fitted by a  $3 \times 10^6$  K thin plasma emission model (Arnaud et al. 1996). BD+30°3639 can be detected because its X-ray emission is attenuated by less than a factor of 10, as shown in Figure 5 (right panel).

The distribution of distances for the ROSAT PN sample is shown in the upper right panel of Figure 6. No PNs further than 1.7 kpc are detected. As extinction usually increases with distance, the lack of detection at large distances is not surprising.

The distributions of the ROSAT PNs with respect to Galactic latitude and Galactic longitude, shown in the right panels of Figure 6, also reflect the effects of absorption. As most of the PNs are in the Galactic plane, the

high-latitude nebulae are nearby and have smaller extinction, while the low-latitude nebulae are in general more distant and have larger extinction. It is thus expected that high-latitude nebulae are easier to detect. The only low-latitude nebula detected is the Dumbbell Nebula, which is located at a small distance, 262 pc. The distribution of the ROSAT PN sample peaks at Galactic longitude = 0. As most of these nebulae are in the Galactic center with several magnitudes of extinction, their non-detection can be expected.

### 3.3. Physical Properties of PNs and X-ray Emission

In order to understand the detectability and emission mechanisms of X-ray emission from PNs, we have included angular radius ( $\theta$ ) and electron density ( $N_e$ ) of the main nebula<sup>3</sup>, effective temperature ( $T_{\text{eff}}$ ) and surface gravity ( $g$ ) of the central star in Table 5. Histograms of the distribution of PNs with respect to nebular density and radius, and stellar effective temperature and surface gravity are presented in Figure 7.

The distributions of PNs detected in X-rays with respect to nebular density and radius (the upper panels of Figure 7) show that the 10 PNs with Type 1 or Type 3 spectra are larger (radius  $> 0.2$  pc) and more tenuous ( $N_e < 300 \text{ cm}^{-3}$ ). As a PN evolves, its radius increases and its density decreases. Since soft X-rays are easily absorbed, evolved PNs are more transparent than younger PNs to the soft X-rays observed in a Type 1 or a Type 3 spectrum because evolved PNs have smaller nebular densities. The three PNs with Type 2 spectra are smaller and denser. These three PNs can be detected because their X-ray spectra are harder and their X-ray emission is less attenuated.

The distributions of PNs with respect to the effective temperature and surface gravity of the central star (the lower panels of Figure 7) show that PNs with Type 1 X-ray spectra have higher stellar effective temperatures and surface gravity. This is expected for photospheric X-ray emission from the hot central stars. On the other hand, PNs with Type 2 spectra have lower stellar effective temperatures and surface gravity, indicating that their emission mechanism must be different from photospheric emission.

### 3.4. Physical Nature of X-ray Emission from PNs

Two types of X-ray emission are detected from PNs: soft X-ray emission whose spectra can be fitted by blackbody models for temperatures of  $1-2 \times 10^5$  K, and harder X-ray emission whose spectra can be fitted by thin plasma emission models of temperatures a few  $10^6$  K. The soft X-ray emission is extremely susceptible to intervening absorption, only sources with absorption column densities  $\ll 10^{21} \text{ cm}^{-2}$  have been detected. The harder X-ray emission is not as attenuated as the soft X-ray emission,

thus can be detected even if the absorption column density reaches  $2 \times 10^{21} \text{ cm}^{-2}$ .

The soft X-ray emission is most likely photospheric emission from the hot central stars. As a PN ages, the nebula expands and becomes more tenuous, while the stellar  $T_{\text{eff}}$  increases and the heavy elements in the stellar atmosphere settle. Therefore, evolved PNs with hot central stars and optically thin nebular shells produce detectable X-ray fluxes. The PNs showing soft X-ray emission all have optically determined stellar properties supporting the photospheric emission explanation.

There are a number of PNs in the ROSAT sample that have stellar effective temperature greater than  $1 \times 10^5$  K but are not detected. These non-detections are mostly caused by high absorption, with  $N_{\text{H}}$  a few times  $10^{21} \text{ cm}^{-2}$ , e.g., A 21, Hb5, K3-92, M3-28, and NGC 6565. Only two non-detections have low absorption column density: A 31 and NGC 1535. The non-detection of A 31 is probably due to the insufficient integration time of the observation, only 1,023 s. NGC 1535 has a dense nebular shell, and its non-detection is probably caused by the absorption in the dense shell.

There might be an additional mechanism to produce soft X-rays from PNs, as illustrated by A 30, which shows only soft X-ray emission below 0.5 keV (Chu & Ho 1995), but diffuse X-ray emission around the bright central source is detected at a  $2\sigma$  level (Chu et al. 1997). A 30 is a large, evolved, "born-again" PN with a very hot central star (Iben et al. 1983); therefore, the point X-ray source at the center is likely photospheric emission from the central star. The marginally detected diffuse emission has a rough spatial correspondence with the radial filaments and bipolar outflows, so it may be produced by interactions between the fast stellar wind and the H-deficient central nebula. The soft spectrum of the diffuse emission implies a very low plasma temperature,  $< 10^6$  K (Chu et al. 1997).

The emission mechanism of the hard X-ray emission from PNs is largely uncertain. In Kwok et al.'s (1978) wind-wind interaction model, the heat conduction between the hot, shocked fast wind and the cold nebular shell would raise the density in the hot gas and produce detectable X-ray emission (Soker 1994). Using this mechanism, Zhekov & Perinotto (1998) have reproduced the spectral properties of NGC 6543 satisfactorily. However, the spatial resolution of the available ROSAT PSPC observations is inadequate to confirm this mechanism morphologically. Among the five PNs showing hard X-ray emission, BD+30°3639, NGC 6543, NGC 7009, NGC 7293, and LoTr 5, only the first two have been marginally resolved by the ROSAT HRI and PSPC, respectively. The X-ray emission might originate within the star, e.g., in the corona (Fleming, Werner, & Barstow 1993) or even in an

<sup>3</sup>We use the radius of the main nebula, instead of the large radius of the outermost features, such as the large halos around BD+30°3639 and NGC 6543, because all X-ray sources in PNs are located within the main nebula and the dense main nebula may absorb soft X-rays significantly

X-ray binary. Future high-resolution observations by the Chandra Observatory would be very useful in determining the emission mechanism of hard X-rays.

Of the five PNs with hard X-ray emission, two also have soft X-ray emission (i.e., Type 3 spectra), LoTr 5 and NGC 7293. These two nebulae, like the PNs with only soft X-ray emission, are large, tenuous, evolved PNs with hot central stars and low extinction. On the other hand, the three nebulae with only hard X-ray emission (i.e., Type 2 spectra) are small, dense, and young, and their central stars are well below  $1 \times 10^5$  K. X-ray luminosities of three PNs with hard X-ray emission have been reported: BD+30°3639 (Type 2) has an X-ray luminosity of  $2-3 \times 10^{32}$  erg s<sup>-1</sup> in the 0.4–1.7 keV band (Arnaud et al. 1996), NGC 6543 (Type 2)  $3 \times 10^{31}$  erg s<sup>-1</sup> in the 0.1–2.4 keV band (Kreysing et al. 1992), and NGC 7293's (Type 3) hard component  $2.6 \times 10^{29}$  erg s<sup>-1</sup> in the 0.1–2.4 keV band (Leahy et al. 1994). It is not clear whether the hard X-ray emission mechanism is the same for these two groups of PNs with contrasting physical properties. It is nevertheless clear that Type 2 spectra could not have resulted from heavily absorbed Type 3 spectra because the central stars of PNs with Type 2 spectra are too cool to produce soft X-ray emission.

As the hard X-rays are not as severely attenuated as the soft X-rays, the small number of hard X-ray sources detected in PNs indicates that hard X-ray emission from PNs is not universal as is the case of soft X-ray emission from a hot photosphere. To understand the nature of hard X-ray emission from PNs, sensitive searches for more sources are needed, and follow-up observations with high spatial and spectral resolution are particularly important.

#### 4. SUMMARY AND CONCLUSIONS

We have used the ROSAT PSPC and HRI archival observations to study X-ray emission from PNs. 63 PNs have useful ROSAT PSPC observations. These observations are used to analyze the spatial and spectral properties of the X-ray emission for positive detections and to determine the  $3\sigma$  upper limits for non-detections. We have examined the effects of absorption and use them to explain the distribution of PNs with detectable X-ray emission with respect to distance, extinction, Galactic latitude and longitude, effective temperature and surface gravity of the central star, and size and density of the nebular shell. The main results are summarized below.

1. 20–25% of the PNs with useful ROSAT PSPC observations show X-ray emission. These include 13 definite detections and 3 possible detections (at a  $2\sigma$  level).
2. Three types of spectra are seen in PNs: Type 1 consists of only soft X-ray emission ( $<0.5$  keV), peaks at 0.1–0.2 keV, and can be fitted by blackbody models at temperatures  $1-2 \times 10^5$  K; Type 2 consists of harder X-ray emission, peaks at  $>0.5$  keV, and can

be fitted by thin plasma emission models at temperatures of a few  $10^6$  K; Type 3 is a composite of a bright Type 1 component and a fainter Type 2 component.

3. The unresolved soft X-ray emission (Type 1 spectra) is most likely photospheric emission from hot central stars. As soft X-ray emission can be severely attenuated by intervening absorption, only large, evolved PNs with hot central stars and small absorption column density,  $\ll 1 \times 10^{21}$  cm<sup>-2</sup>, are detected.
4. Marginally resolved soft X-ray emission is detected in the evolved, H-deficient PN A 30. Its central bright point X-ray source is probably photospheric emission, and the surrounding diffuse emission (at a  $2\sigma$  level) may result from the interaction between the fast stellar wind and the surrounding medium.
5. The origin of the hard X-ray emission (Type 2 spectra and the hard component of Type 3 spectra) is uncertain. It could originate in a stellar corona, X-ray binary, or shocked stellar wind. As hard X-ray emission is not as easily attenuated as soft X-ray emission, the small number of hard X-ray emitting PNs implies a real paucity of hard X-ray sources among PNs.
6. PNs with Type 2 spectra and PNs with Type 3 spectra exhibit different stellar and nebular properties. The former are associated with small, dense, young PNs with relatively cool ( $\ll 10^5$  K) central stars, while the latter are associated with large, tenuous, evolved PNs with hot ( $\leq 10^5$  K) central stars. These two groups of PNs may have different emission mechanisms for their hard X-rays.
7. Among PNs showing hard X-ray emission (Type 2 or Type 3), only two are marginally resolved, BD+30°3639 and NGC 6543, both with Type 2 spectra. The X-ray luminosities of these PNs are  $10^2 - 10^3$  times higher than that of the hard component of NGC 7293, whose spectrum is of Type 3. Observations with high spatial resolution are necessary to determine the origin of their hard X-ray emission.

This work is supported by the NASA grant NAG 5-8103 (ADP). MAG is supported partially by the Dirección General de Enseñanza Superior e Investigación Científica of the Spanish Ministry of Education and Culture. This research has made use of data obtained through the High Energy Astrophysics Science Archive Research Center Online Service, provided by the NASA/Goddard Space Flight Center.

## APPENDIX

## NOTES ON INDIVIDUAL OBJECTS

**PN G 036.1–57.1 = NGC 7293 = Helix Nebula**

Despite the large angular size ( $\sim 960'$ ) of the nebula, its X-ray emission is unresolved and coincident with the position of the central star. Its X-ray spectrum, Type 3, cannot be fitted by one single component; two components are needed. The soft component is most likely the photospheric emission from the hot central star, but the origin of the hard component is less certain (Leahy et al. 1994).

**PN G 037.7–34.5 = NGC 7009 = Saturn Nebula**

The Saturn Nebula has an elliptical ( $25'' \times 10''$ ) main nebula with two ansae extending out to  $25''$  from the central star. The total number of PSPC counts detected is too low to determine reliably whether the X-ray emission is from a point source or is extended. While the PSPC spectrum is too noisy for spectral fits, it shows that most of the detected X-ray photons have energies greater than 0.5 keV, indicating that the X-ray emission probably originates from a hot plasma, instead of the stellar photosphere. Future observations with higher spatial and spectral resolution are needed to determine the real nature of the Saturn Nebula's X-ray emission.

**PN G 060.8–03.6 = NGC 6853 = Dumbbell Nebula**

The Dumbbell Nebula is the brightest X-ray source among PNs known to emit X-rays. Its X-ray emission appears extended in PSPC images extracted from energies below 0.2 keV (Kreysing et al. 1992) owing to an electronic ghost image problem (Chu et al. 1993). The PSPC images extracted at energies greater than 0.2 keV and the HRI image both show only a point source at the position of the central star. The PSPC spectrum peaks at the lowest energy bins. These spatial and spectral properties indicate that the X-ray emission from the Dumbbell Nebula originates in the central star's photosphere.

**PN G 064.7+05.0 = BD+30°3639**

BD+30°3639 is very likely a young PN because of its small ( $\sim 4'' = 0.04$  pc), dense nebular shell and the low temperature of its central star (Harrington et al. 1997). Its X-ray spectrum can be fitted by a thin plasma emission model for a temperature of  $3 \times 10^6$  K (Kreysing et al. 1992; Arnaud et al. 1996). The observed X-rays cannot be explained by stellar photospheric emission. Leahy et al. (1998) analyzed an HRI image of BD+30°3639 and reported that the X-ray emission is marginally extended for a resolution of  $\sim 5''$ . It is possible that the X-ray emission of BD+30°3639 is from the hot plasma in the central cavity of the PN shell, but high-resolution observations in the future are needed to confirm this result.

**PN G 094.0+27.4 = K 1-16**

K 1-16 is an extended ( $90'' \times 70''$ ) low surface brightness nebula (Manchado et al. 1996) with a He-rich PG1159 type central star. Its X-ray spectral distribution is compatible with the stellar photospheric emission of its hot central star (Hoare et al. 1995).

K 1-16 is projected within a cluster of galaxies and  $\sim 2'$  from the QSO E1821+643 (Saxton et al. 1997). As the X-ray emission from the PN is superposed on the extended emission from the cluster of galaxies, the extraction of X-ray emission from the PN is somewhat difficult. For background subtraction, we have chosen background regions with similar surface brightness around the QSO. The resultant X-ray spectrum of K 1-16 (Figure 3) does not show any significant emission at 1.0 keV, where the QSO spectrum peaks. Therefore, the background subtraction is probably reasonable and the QSO contamination of the PN spectrum at the soft 0.1–0.3 keV band is probably negligible.

**PN G 096.4+29.9 = NGC 6543 = Cat's Eye**

ROSAT PSPC observations of this PN show extended X-ray emission, and the PSPC spectrum is best fitted by thin plasma emission models for temperatures of a few  $10^6$  K (Kreysing et al. 1992). This nebula is thus the best candidate for follow-up study of diffuse X-ray emission from PNs. The optical size of the bright central nebula ( $\sim 26'' \times 18''$ ) matches roughly the PSPC resolution. High-resolution observations with Chandra should reveal clearly the distribution of X-ray emission and its relationship with the optical morphological features, allowing us to determine the nature of the X-ray emission.

**PN G 118.8–74.7 = NGC 246**

NGC 246 is a very extended ( $\sim 5' \times 6'$ ) low surface brightness nebula. Its central star is also a member of the He-rich PG1159 class of pre-white dwarfs, similar to the central star of K 1-16. The central star of NGC 246 is a binary (Cudworth 1973) with a companion widely separated by 1900 AU (Howard & Ciardullo 1999). The X-ray emission from NGC 246 is consistent with that expected from the photosphere of the hot central star. It is unnecessary to assume an X-ray binary to explain the X-ray emission.

**PN G 143.6+23.8 = EGB 4**

As already noted in §2, the PN classification for EGB 4 is uncertain. Bright X-ray emission is detected from its central

star BZ Cam, a white dwarf in a cataclysmic binary system. The spectral distribution of the X-ray emission is consistent with such a binary system (van Teeseling & Verbunt 1994).

**PN G 148.4+57.0 = NGC 3587 = Owl Nebula**

The PSPC X-ray spectrum of the Owl Nebula was reported by Leahy et al. (1996); however, the double-hump spectral shape was caused by the inclusion of a background source. ROSAT HRI observations of the Owl Nebula clearly show two point sources projected within the nebula, and both sources have a stellar counterpart. One source is coincident with the position of the central star and its PSPC spectrum shows only photons with energies below 0.5 keV, consistent with the photospheric emission expected from the hot central star. The other source is probably associated with a background star; its PSPC spectrum is similar to those of stellar coronal emission. A detailed description of the X-ray sources has been reported by Chu et al. (1998).

**PN G 198.6–06.3 = A 12**

The X-ray emission from A 12 reported by Kreysing et al. (1992) was misidentified. As shown in Figure 2 and pointed out by Hoare et al. (1995), the X-ray source is coincident in position with the bright binary star  $\mu$  Ori located  $\sim 1'$  from A 12 (Hoare et al. 1995). No X-ray emission is evident at the position of A 12.

**PN G 206.4–40.5 = NGC 1535**

X-ray emission from NGC 1535 has been reported by Apparao & Tarafdar (1989) using EXOSAT observations and by Leahy et al. (1996) using ROSAT PSPC observations. A comparison between optical and PSPC X-ray images reveals that the X-ray source is outside the optical boundary of NGC 1535, and appears to be associated with a field star. The previously reported X-ray emission from NGC 1535 is therefore mis-identified; no X-ray emission is detected within the optical boundary of NGC 1535 (Chu et al. 1998).

**PN G 208.5+33.2 = A 30**

A 30 contains a H-deficient central nebula and a large halo. The X-ray emission was serendipitously discovered by Chu & Ho (1995) using a ROSAT PSPC observation centered on a cluster of galaxies. Subsequent HRI observations confirm the detection and reveal a marginally extended X-ray source at the central H-deficient nebula (Chu et al. 1997). Unfortunately, the X-ray emission from A 30 is too faint and too soft for Chandra, and is too small for XMM.

**PN G 220.3–53.9 = NGC 1360**

NGC 1360 is the first PN reported to emit X-rays (de Korte et al. 1985). Its optical nebula is extended ( $\sim 5.5' \times 3'$ ) and has a low surface brightness. The unresolved X-ray emission from NGC 1360 is coincident in position with the central star, and the X-ray spectrum can be modeled as photospheric emission from a hot star (Hoare et al. 1995).

**PN G 238.0+34.8 = A 33**

The X-ray emission from A 33 was reported by Tarafdar & Apparao (1988) using Einstein observations. As in the cases of A 12 and NGC 1535, a comparison between optical and PSPC X-ray images (see Figure 2) shows that the X-ray source is outside the optical nebula of A 33. The previously reported X-ray emission from A 33 is therefore spurious (Conway & Chu 1997).

**PN G 286.8–29.5 = K 1-27**

K 1-27 is an elliptical ( $65'' \times 50''$ ) PN with a low surface brightness. The total number of PSPC counts detected is too low to allow detailed spatial or spectral analysis. The PSPC spectrum does not peak in the lowest energy channels as have other spectra attributed to photospheric emission from hot stars (e.g., NGC 246 and NGC 1360). Deeper observations with higher spatial resolution are needed to determine the spatial distribution and spectral properties of the X-ray emission from K 1-27.

**PN G 318.4+41.4 = A 36**

A 36 is an extended ( $\sim 8' \times 5'$ ) nebula with a low surface brightness. Leahy et al. (1996) reported the PSPC X-ray spectrum of A 36; however, their extracted spectrum included the contribution of a background source projected near the northern boundary of the nebula (see Figure 2). Using a small aperture that includes only the X-ray source at the central star of A 36, we have extracted a PSPC spectrum. This spectrum shows only photons with energies below 1 keV, but does not peak in the lowest energy channels as the spectra from objects interpreted as photospheric emission from hot stars. Deeper observations are needed to determine the spatial and spectral properties of the X-ray emission from A 36.

**PN G 339.9+88.4 = LoTr 5**

LoTr 5 is an extended ( $\sim 17'$ ), nearby PN of extremely low surface brightness. Its central star is known to be a binary (perhaps even triple) system (Jasniewicz et al. 1996, and references therein). The X-ray spectrum of LoTr 5 is similar to that of the Helix Nebula, consisting of a strong soft component and a weak harder component.



## REFERENCES

- Acker, A., Ochsenbein, F., Stenholm, B., Tylanda, R., Marcout, J., & Schohn, C. 1992, Strasbourg-ESO Catalogue of Galactic Planetary Nebulae (Strasbourg: ESO)
- Apparao, K. M. V., & Tarafdar, S. P. 1989, *ApJ*, 344, 826
- Arnaud, K., Borkowski, K. J., & Harrington, J. P. 1996, *ApJ*, 462, L75
- Bohlin, R. C., Savage, B. D., & Drake, J. F. 1978 *ApJ*, 224, 132
- Cahn, J. H., Kaler, J. B., & Stanghellini, L. 1992, *ApJS*, 94, 399
- Chu, Y.-H., Chang, T. H., Conway, G. M. 1997, *ApJ*, 482, 891
- Chu, Y.-H., Gruendl, R. A., & Conway, G. M. 1998, *AJ*, 116, 1882
- Chu, Y.-H., & Ho, C.-H. 1995, *ApJ*, 448, L127
- Chu, Y.-H., Kwitter, K., & Kaler, J. 1993, *AJ*, 106, 650
- Conway, G. M., & Chu, Y.-H. 1997, in *IAU Symp. 180, Planetary Nebulae*, eds. H. J. Habing, & H. J. G. L. M. Lamers (Dordrecht: Kluwer), 214
- Corradi, R. L. M. 1995, *MNRAS*, 276, 521
- Crawford, I. A., & Barlow, M. J. 1991, *A&A*, 249, 518
- Cudworth, K. 1973, *PASP*, 85, 401
- David, L. P., Harnden, F. R., Jr., Kearns, K. E., & Zombeck, M. V. 1996, *The ROSAT High Resolution Imager (HRI) Calibration Report* (Cambridge: SAO)
- de Freitas, Pacheco, J. A., Codina, S. J., & Viadana, L. 1986, *MNRAS*, 220, 107
- de Korte, P. A. J., Claas, J. J., Jansen, F. A., & McKechnie, S. P. 1985, *AdSpR*, 5, 57
- Fleming, T. A., Werner, K., & Barstow, M. A. 1993, *ApJ*, 416, L79
- Fruscione, A., Drake, J. J., McDonald, K., & Malina, R. F. 1995, *ApJ*, 441, 726
- Gleizes, F., Acker, A., & Stenholm, B. 1989, *A&A*, 222, 237
- Harrington J. P., Lame, N. J., White, S. M., & Borkowski, K. J. 1997, *AJ*, 113, 2147
- Hoare, M. G., Martin, A. B., Werner, K., & Fleming, T. 1995, *MNRAS*, 273, 812
- Hollis, J. M., Oliverson, R. J., Wagner, R. M., & Feibelman, W. A. 1992, *ApJ*, 393, 217
- Howard, B. E., & Ciardullo, R. 1999, *PASP*, 111, 217
- Iben, I. Jr., Kaler, J. B., Truran, J. W., & Renzini, A. 1983, *ApJ*, 264, 605
- Jasniewicz, G., Thévenin, F., Monier, R., & Skiff, B. A. 1996, *A&A*, 307, 200
- Kaler, J. B. 1983, *ApJ*, 271, 188
- Kraft, R. P., Krzeminski, W., & Mumford, G. S. 1969, *ApJ*, 158, 589
- Kreysing, H. C., Diesch, C., Zweigle, J., Staubert, R., Grewing, M., & Hasinger, G. 1992, *A&A*, 264, 623
- Leahy, D. A., Kwok, S., & Yin, D. 1998, *AAS*, 192, 895
- Leahy, D. A., Zhang, C. Y., & Kwok, S. 1994, *ApJ*, 422, L205
- Manchado, A., Guerrero, M. A., Stanghellini, L., & Serra-Ricart, M. 1996, *The IAC Morphological Catalog of Northern Galactic Planetary Nebulae*, IAC Publ., Tenerife
- McCarthy, J. K., Mould, J. R., Méndez, R. H., Kudritzki, R. P., Husfeld, D., Herrero, A., & Groth, H. G. 1990, *ApJ*, 351, 230
- Méndez, R. H., Kudritzki, R. P., Herrero, A., Husfeld, D., & Groth, H. G. 1988, *A&A*, 190, 113
- Morrison, R., & McCammon, D. 1983, *ApJ*, 270, 119
- Phillips, J. P. 1988, *A&A*, 340, 527
- Rauch, T., Koeppen, J. & Werner, K. 1994, *A&A*, 286, 543
- Raymond, J. C., & Smith, B. W. 1977, *ApJS*, 35, 419
- ROSAT Mission Description 1991, NASA Publ. NRA 91-OSSA-25, Appendix F
- Saxton, R. D., Barstow, M. A., Turner, M. J. L., Williams, O. R., Stewart, G. C., & Kii, T. 1997, *MNRAS*, 289, 196
- Shaw, R. A., & Kaler, J. B. 1989, *ApJS*, 69, 495
- Soker, N. 1994, *AJ*, 107, 276
- Tarafdar, S. P., & Apparao, K. M. V. 1988, *ApJ*, 327, 342
- Tylanda, R., Acker, A., Stenholm, B., & Köpper, J. 1992, *A&AS*, 95, 337
- van Teeseling, A. & Verbunt, F. 1994, *A&A*, 292, 519
- Zhekov, S. A., & Perinotto, M. 1998, *A&A*, 334, 239

TABLE 1  
 ROSAT PSPC AND HRI POINT OBSERVATIONS OF PNE

PN G	PN Name	ROSAT Obs.	Exp. Time [s]	Offset [']
000.1-01.1	M 3-43	rp400201n00	2202	11
000.1+02.6	Al 2-J	rp900204n00	3662	6
		rh900394n00	4901	5
000.5-01.6	Al 2-Q	rp400209n00	2349	19
000.6-01.3	Bl 3-15	rp400209n00	2349	4
000.7-03.7	M 3-22	rp600418n00	29578	20
000.8-01.5	Bl O	rp400209n00	2349	19
001.2-03.9	ShWi 2-5	rp600418n00	29578	10
002.2+00.5	Te 2337	rp900199n00	4716	14
		rp900199a01	1784	14
002.6-03.4	M 1-37	rp201093n00	10033	8
003.3-07.5	KFL 19	rp400054m01	5296	7
003.5-04.6	NGC 6565	rp300188n00	9980	20
003.8-04.3	H 1-59	rp300188n00	9980	15
003.9+01.6	Te 2111	rh300060n00	22543	7
004.5+06.8	H 2-12	rp500050n00	1784	1
		rh500099n00	36662	1
007.8-03.7	M 2-34	rp500009n00	3992	5
009.8-07.5	GJC 1	rp300058n00	8295	0
		rh300184a01	31709	0
019.9+00.9	M 3-53	rp400326n00	11796	10
021.7-00.6	M 3-55	rp500287n00	9100	5
		rp500287a01	5996	5
021.8-00.4	M 3-28	rp500287n00	9100	1
031.9-00.3	WeSb 4	rp900402n00	23825	19
034.6+11.8	NGC 6572	rp200673n00	4442	0
		rh200145n00	3463	0
036.1-57.1	NGC 7293	rp900187n00	4914	0
037.7-34.5	NGC 7009	rp200672n00	4367	0
		rh200141n00	3772	0
039.5-02.7	M 2-47	rp500058a02	20575	17
		rp500058a01	18484	17
		rp500058a00	5010	17
040.4-03.1	K 3-30	rp200126n00	7194	8
043.1+37.7	NGC 6210	rh200144n00	5611	0
049.3+88.1	H 4-1	rp800006n00	21545	10
053.3+03.0	A 59	rh201632n00	1752	3
053.8-03.0	A 63	rp201100n00	6726	20
060.8-03.6	NGC 6853	rp900016n00	5905	0
		rp200568n00	5242	0
		rp200568a01	5155	0
		rp200568a02	3621	0
		rh200569a01	3573	0
061.4-09.5	NGC 6905	rh201101n00	17578	0
064.7+05.0	BD+30 3639	rp201096n00	5834	0
		rp500327n00	3686	17
		rh900709n00	8740	0
065.0-27.3	Ps 1	rp400081n00	8780	0
		rh400611n00	52468	0

TABLE 1—*Continued*

PN G	PN Name	ROSAT Obs.	Exp. Time [s]	Offset [']
068.7+01.9	K 4-41	rp201102n00	7941	1
068.7+03.0	PC 23	rp400048a00	5065	15
076.3+01.1	A 69	rp200062n00	13811	19
		rp200063n00	2055	19
		rp200058n00	1913	19
		rp200057n00	1826	19
077.5+03.7	KjPn 1	rp500208n00	2302	13
077.7+03.1	KjPn 2	rp500207n00	9310	19
088.7+04.6	K 3-78	rp500220n00	4895	18
094.0+27.4	K 1-16	rp700413n00	1128	0
		rp700948n00	1980	0
		rp700949n00	1858	0
		rh800754n00	29427	1
096.4+29.9	NGC 6543	rp000026n00	44989	9
		rp170075n00	41204	15
		rh120030n00	47482	9
104.2–29.6	Jn 1	rp200122n00	1140	0
		rf200122n00	4192	0
110.6–12.9	K 1-20	rp900343n00	8838	16
118.8–74.7	NGC 246	rf200842n00	7471	0
		rf200842a01	3962	0
130.4+03.1	K 3-92	rp180068n00	5826	14
148.4+57.0	NGC 3587	rp900186n00	1783	0
		rh900706n00	35224	0
166.4–06.5	CRL 618	rh201614n00	18697	0
183.8+05.5	WeSb 2	rp300191n00	17255	14
189.1+19.8	NGC 2371-72	rp200450n00	11758	0
197.8+17.3	NGC 2392	rp500112n00	3795	19
198.6–06.3	A 12	rp201097n00	10287	0
		rh201866n00	4923	0
205.1+14.2	A 21	rp200121a01	1628	0
		rp200121a00	1192	0
206.4–40.5	NGC 1535	rp900242n00	11620	0
208.5+33.2	A 30	rp800370n00	21773	11
		rh900643n00	55795	0
215.2–24.2	IC 418	rp200676n00	5085	0
		rh200671n00	6040	0
219.1+32.2	A 31	rp200120n00	1023	0
220.3–53.9	NGC 1360	rf200843n00	8722	0
233.5–16.3	A 15	rp201071n00	4439	3
238.0+34.8	A 33	rp200119a01	1526	1
		rp200119n00	1205	1
260.7–03.3	Wray 16-20	rp500055a01	1725	10
		rp500055n00	1215	10
		rh500164n00	3822	0
285.4+01.5	Pe 1-1	rp400394n00	1196	8
286.8–29.5	K 1-27	rp201245n00	18447	0
288.8–05.2	He 2-51	rp200868n00	2676	15
		rp200863n00	2264	12

TABLE 1—*Continued*

PN G	PN Name	ROSAT Obs.	Exp. Time [s]	Offset [']
296.5–06.9	He 2-71	rh180140n00	1174	11
		rh180141n00	2155	15
318.4+41.4	A 36	rp900244n00	9992	0
322.4–00.1	Pe 2-8	rp500160n00	4770	5
326.1–01.9	VBe 3	rp500010n00	3904	11
339.9+88.4	LoTr 5	rp201514n00	18788	0
346.3–06.8	Fg 2	rp400077n00	20937	17
347.7+02.0	Vd 1-8	rh400706n00	2467	8
352.9–07.5	Fg 3	rp300042n00	5605	11
355.9–04.2	M 1-30	rp201383n00	28760	14
		rp200983a01	26361	15
		rp200983n00	22287	15
357.1–04.7	H 1-43	rp400269n00	21168	5
357.6+01.0	TrBr 4	rh300062n00	2638	9
358.8–00.0	Te 2022	rp400275n00	15517	17
		rp400275a01	13229	17
359.2+01.2	19W32	rp400186n00	2100	9
359.3+01.4	Th 3-35	rp400186n00	2100	5
		rh400747n00	11922	14
359.3–00.9	Hb 5	rp400179n00	2082	6
		rh400177n00	3675	1
359.8+02.4	Th 3-33	rp900204n00	3662	16
359.8–07.2	M 2-32	rp200916n00	4581	11

TABLE 2  
PNE WITH DETECTED X-RAY EMISSION IN ROSAT PSPC OBSERVATIONS

PN G	PN Name	Count number [counts]	X-ray flux [count s <sup>-1</sup> ]	3- $\sigma$ [count s <sup>-1</sup> ]	Spectral Type
036.1-57.1	NGC 7293	300±20	0.06	0.012	Type 3
037.7-34.5	NGC 7009	24± 7	0.005	0.005	Type 2 ?
060.8-03.6	NGC 6853	7700±90	0.39	0.014	Type 1
064.7+05.0	BD+30 3639	420±25	0.044	0.007	Type 2
094.0+27.4	K 1-16	200±17	0.04	0.010	Type 1
096.4+29.9	NGC 6543	560±30	0.0065	0.0011	Type 2
118.8-74.7	NGC 246	1050±35	0.091	0.009	Type 1
148.4+57.0	NGC 3587	14± 5	0.008	0.009	Type 1
208.5+33.2	A 30	109±16	0.005	0.0022	Type 1
220.3-53.9	NGC 1360	111±16	0.013	0.006	Type 1
286.8-29.5	K 1-27	34±10	0.0018	0.0016	Type 2 ?
318.4+41.4	A 36	31± 8	0.003	0.0023	Type 2 ?
339.9+88.4	LoTr 5	420±25	0.022	0.004	Type 3

TABLE 3  
PNE TENTATIVELY DETECTED IN ROSAT PSPC OBSERVATIONS

PN G	PN Name	Count number [counts]	X-ray flux [count s <sup>-1</sup> ]	3- $\sigma$ [count s <sup>-1</sup> ]
034.6+11.8	NGC 6572	8± 5	0.0018	0.003
189.1+19.8	NGC 2371-72	23±14	0.0020	0.004
197.8+17.3	NGC 2392	8± 5	0.0021	0.004

TABLE 4  
PNE UNDETECTED IN ROSAT PSPC OBSERVATIONS

PN G	PN Name	$3\text{-}\sigma$ [count s <sup>-1</sup> ]	PN G	PN Name	$3\text{-}\sigma$ [count s <sup>-1</sup> ]
000.1-01.1	M 3-43	0.004	077.5+03.7	KjPn 1	0.0025
000.1+02.6	Al 2-J	0.003	077.7+03.1	KjPn 2	0.0012
000.5-01.6	Al 2-Q	0.003	088.7+04.6	K 3-78	0.0014
000.6-01.3	Bl 3-15	0.006	104.2-29.6	Jn 1	0.03
000.7-03.7	M 3-22	0.0006	110.6-12.9	K 1-20	0.0015
000.8-01.5	Bl O	0.004	130.4+03.1	K 3-92	0.0012
001.2-03.9	ShWi 2-5	0.0009	183.8+05.5	WeSb 2	0.0024
002.2+00.5	Te 2337	0.0020	205.1+14.2	A 21	0.03
002.6-03.4	M 1-37	0.0015	206.4-40.5	NGC 1535	0.0016
003.3-07.5	KFL 19	0.0022	215.2-24.2	IC 418	0.0022
003.5-04.6	NGC 6565	0.0013	219.1+32.2	A 31	0.04
003.8-04.3	H 1-59	0.0017	233.5-16.3	A 15	0.0016
007.8-03.7	M 2-34	0.003	238.0+34.8	A 33	0.007
009.8-07.5	GJJC 1	0.0020	285.4+01.5	Pe 1-1	0.007
019.9+00.9	M 3-53	0.0012	326.1-01.9	VBe 3	0.003
021.7-00.6	M 3-55	0.0008	346.3-06.8	Fg 2	0.0014
021.8-00.4	M 3-28	0.0014	352.9-07.5	Fg 3	0.0024
031.9-00.3	WeSb 4	0.0010	358.8-00.0	Te 2022	0.0006
039.5-02.7	M 2-47	0.0006	359.2+01.2	19W32	0.005
040.4-03.1	K 3-30	0.0019	359.3+01.4	Th 3-35	0.006
053.8-03.0	A 63	0.0020	359.3-00.9	Hb 5	0.005
068.7+01.9	K 4-41	0.0020	359.8+02.4	Th 3-33	0.003
068.7+03.0	PC 23	0.0023	359.8-07.2	M 2-32	0.003
076.3+01.1	A 69	0.0012			

TABLE 5  
PLANETARY NEBULAE PARAMETERS

PN G Name <i>l</i> <i>b</i>	PN Name	<i>d</i> [pc]	<i>A<sub>V</sub></i> [mag]	<i>N<sub>H</sub></i> [10 <sup>21</sup> cm <sup>-2</sup> ]	<i>θ</i> [ $''$ ]	<i>N<sub>e</sub></i> [cm <sup>-3</sup> ]	<i>T<sub>eff</sub></i> [K]	log( <i>g</i> )
000.1-01.1	M 3-43	5819	7.8	14.4	1.9	1550	...	...
000.1+02.6	AI 2-J	...	...	...	...	...	...	...
000.5-01.6	AI 2-Q	...	...	...	...	...	...	...
000.6-01.3	BI 3-15	...	8.3	15.2	...	...	...	...
000.7-03.7	M 3-22	7641	2.1	3.8	3.2	...	104500	5.5
000.8-01.5	BIO	...	4.0	7.4	...	...	...	...
001.2-03.9	ShWi 2-5	...	2.5	4.6	...	...	90000 <sup>1</sup>	...
002.2+00.5	Te 2337	...	...	...	...	...	...	...
002.6-03.4	M 1-37	5830	2.5	4.6	1.4	4000	37800	3.7
003.3-07.5	KFL 19	...	1.1	2.0	...	...	...	...
003.5-04.6	NGC 6565	4616	0.9	1.7	4.5	1460	144000	7.3
003.8-04.3	H 1-59	9348	2.2	4.0	3.0	1350	...	...
007.8-03.7	M 2-34	...	3.7	6.8	...	...	...	...
009.8-07.5	GJJC 1	...	...	...	...	...	...	...
019.9+00.9	M 3-53	...	6.9	12.8	...	...	...	...
021.7-00.6	M 3-55	...	5.2	9.6	3.6	...	...	...
021.8-00.4	M 3-28	4856	6.3	11.6	4.5	...	130500	5.8
031.9-00.3	WeSb 4	...	...	...	...	...	...	...
034.6+11.8	NGC 6572	705	0.7	1.4	7.2	4960	56900 <sup>2</sup>	...
036.1-57.1	NGC 7293	157	0.09	0.16	402.0	160	100000	6.9
037.7-34.5	NGC 7009	1201	0.24	0.44	14.1	3860	82000 <sup>3</sup>	4.8
039.5-02.7	M 2-47	4743	3.8	7.0	4.1	2750	...	...
040.4-03.1	K 3-30	6291	4.0	7.3	1.7	...	...	...
053.8-03.0	A 63	...	2.6	4.8	...	...	...	...
060.8-03.6	NGC 6853	262	0.4	0.7	170.0	250	110100	7.3
064.7+05.0	BD+30°3639	1162	1.0	1.8	2.4	10000	31100	3.1
068.7+01.9	K 4-41	7929	3.5	6.4	1.5	...	...	...
068.7+03.0	PC 23	6680	3.7	6.8	1.1	...	...	...
076.3+01.1	A 69	4173	4.9	9.0	11.0	...	...	...
077.5+03.7	KjPn 1	...	3.7	6.8	...	...	...	...
077.7+03.1	KjPn 2	...	...	...	...	...	...	...
088.7+04.6	K 3-78	7831	...	...	2.2	...	...	...
094.0+27.4	K 1-16	1003	0.0	0.0	47.0	102 <sup>4</sup>	138000 <sup>5</sup>	6.1
096.4+29.9	NGC 6543	982	0.3	0.5	9.4	2700	47000	3.8
104.2-29.6	Jn 1	709	0.6	1.1	166.0	15 <sup>4</sup>	95000	...
110.6-12.9	K 1-20	4178	1.1	2.0	17.0	...	...	...
118.8-74.7	NGC 246	629	0.3	0.5	112.0	200 <sup>4</sup>	85000 <sup>3</sup>	5.7
130.4+03.1	K 3-92	6806	3.0	5.5	6.5	130	115000	...
148.4+57.0	NGC 3587	615	0.02	0.04	100.0	125	104000	...
183.8+05.5	WeSb 2	...	...	...	...	...	...	...
189.1+19.8	NGC 2371-72	1539	0.3	0.5	21.8	1700	68300	5.1
197.8+17.3	NGC 2392	1149	0.5	0.9	22.4	1280	47000 <sup>6</sup>	3.8
205.1+14.2	A 21	243	0.0	0.0	307.5	180	137000	...
206.4-40.5	NGC 1535	2283	0.22	0.40	9.2	2140	138000 <sup>3</sup>	6.5
208.5+33.2	A 30	1689	0.0	0.0	63.5	20	116000	5.5
215.2-24.2	IC 418	609	0.7	1.2	6.2	4100	36000	3.5
219.1+32.2	A 31	233	0.0	0.0	486.0	10 <sup>4</sup>	147000	...
220.3-53.9	NGC 1360	350	0.0	0.0	192.0	100	80000 <sup>3</sup>	5.4
233.5-16.3	A 15	3656	0.22	0.4	17.0	50	65000 <sup>3</sup>	4.1

TABLE 5—*Continued*

PN G Name <i>l b</i>	PN Name	<i>d</i> [pc]	<i>A<sub>V</sub></i> [mag]	<i>N<sub>H</sub></i> [10 <sup>21</sup> cm <sup>-2</sup> ]	<i>θ</i> [″]	<i>N<sub>e</sub></i> [cm <sup>-3</sup> ]	<i>T<sub>eff</sub></i> [K]	log( <i>g</i> )
238.0+34.8	A 33	751	0.8	1.5	134.0	30 <sup>4</sup>	86000 <sup>1</sup>	...
285.4+01.5	Pe 1-1	2219	3.9	7.2	1.5	10940	78000 <sup>7</sup>	...
286.8-29.5	K 1-27	1300	0.15	0.28	53.0	50 <sup>8</sup>	110000	6.5
318.4+41.4	A 36	243	0.22	0.40	183.5	36 <sup>4</sup>	95000 <sup>6</sup>	5.3
326.1-01.9	VBe 3	...	2.6	4.8	...	...	...	...
339.9+88.4	LoTr 5	616	0.0	0.00	510	20	150000	...
346.3-06.8	Fg 2	...	1.1	2.1	...	...	...	...
352.9-07.5	Fg 3	2249	1.5	2.8	1.0	...	49000 <sup>7</sup>	...
358.8-00.0	Te 2022	...	...	...	...	...	...	...
359.2+01.2	19W32	...	6.3 <sup>9</sup>	11.6	23.0	...	...	...
359.3+01.4	Th 3-35	...	6.5	12.0	...	...	...	...
359.3-00.9	Hb 5	1242	4.1	7.5	10.0	6280	131000	5.9
359.8+02.4	Th 3-33	...	7.6	14.0	...	...	...	...
359.8-07.2	M 2-32	...	0.9	1.6	...	...	60000 <sup>7</sup>	...

REFERENCES.—All data come from Cahn, Kaler, & Stanghellini (1992) unless otherwise marked with one of the following superscripts: (1) Shaw & Kaler (1989); (2) de Freitas et al (1986); (3) Méndez et al. (1988); (4) Phillips (1988); (5) Kaler (1983); (6) McCarthy et al. (1990); (7) Gleizes, Acker, & Stenholm (1989); (8) Rauch, Köppen, & Werner (1994); and (9) Corradi (1995).



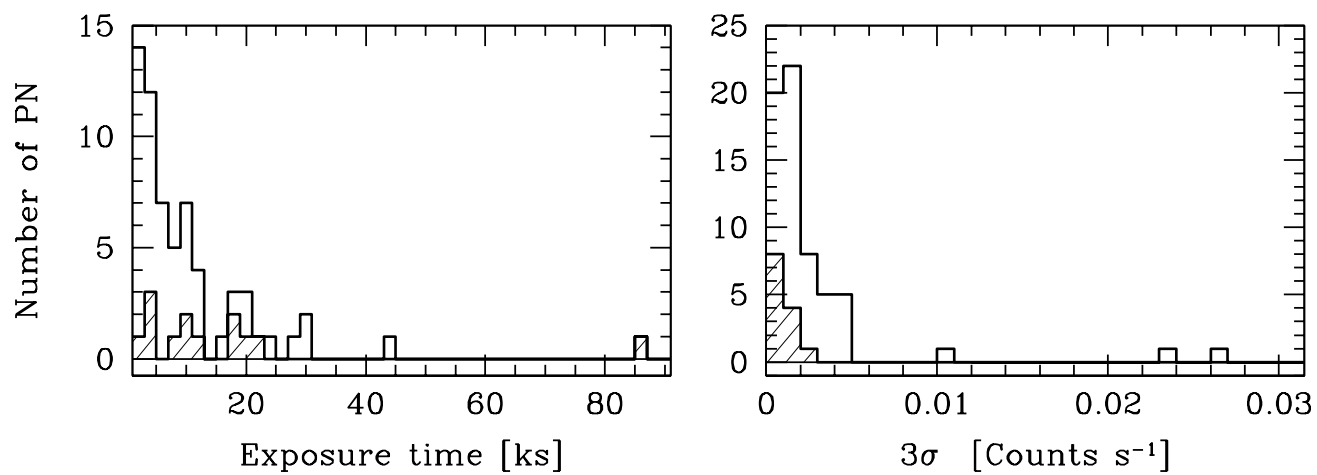


FIG. 1— Observed distributions of the exposure time [*left*] and  $3\sigma$  detection limit [*right*] measured for the PSC observations of the ROSAT PN sample. The sample size is 63 PNs, and the number of detections is 13 PNs. The shaded portion of the histograms show the distribution of detected PNs.

FIG. 2*a*– X-ray [*left*] and Digital Sky Survey [*right*] images of NGC 7293, NGC 7009, and NGC 6853. Contours of the X-ray emission are overlaid on both images. The contour levels are 20, 50, 75, and 90% of the peak surface brightness of the PN X-ray emission.

FIG. 2*b*– Same as Fig. 2*a*, but for BD+30°3639, K 1-16, and NGC 6543.

FIG. 2*c*– Same as Fig. 2*a*, but for NGC 246, NGC 3587, and A 12 (previously misidentified as the source of nearby X-ray emission).

FIG. 2*d*– Same as Fig. 2*a*, but for A 30, NGC 1360, and A 33 (previously misidentified as the source of nearby X-ray emission).

FIG. 2*e*– Same as Fig. 2*a*, but for K 1-27, A 36, and LoTr 5.

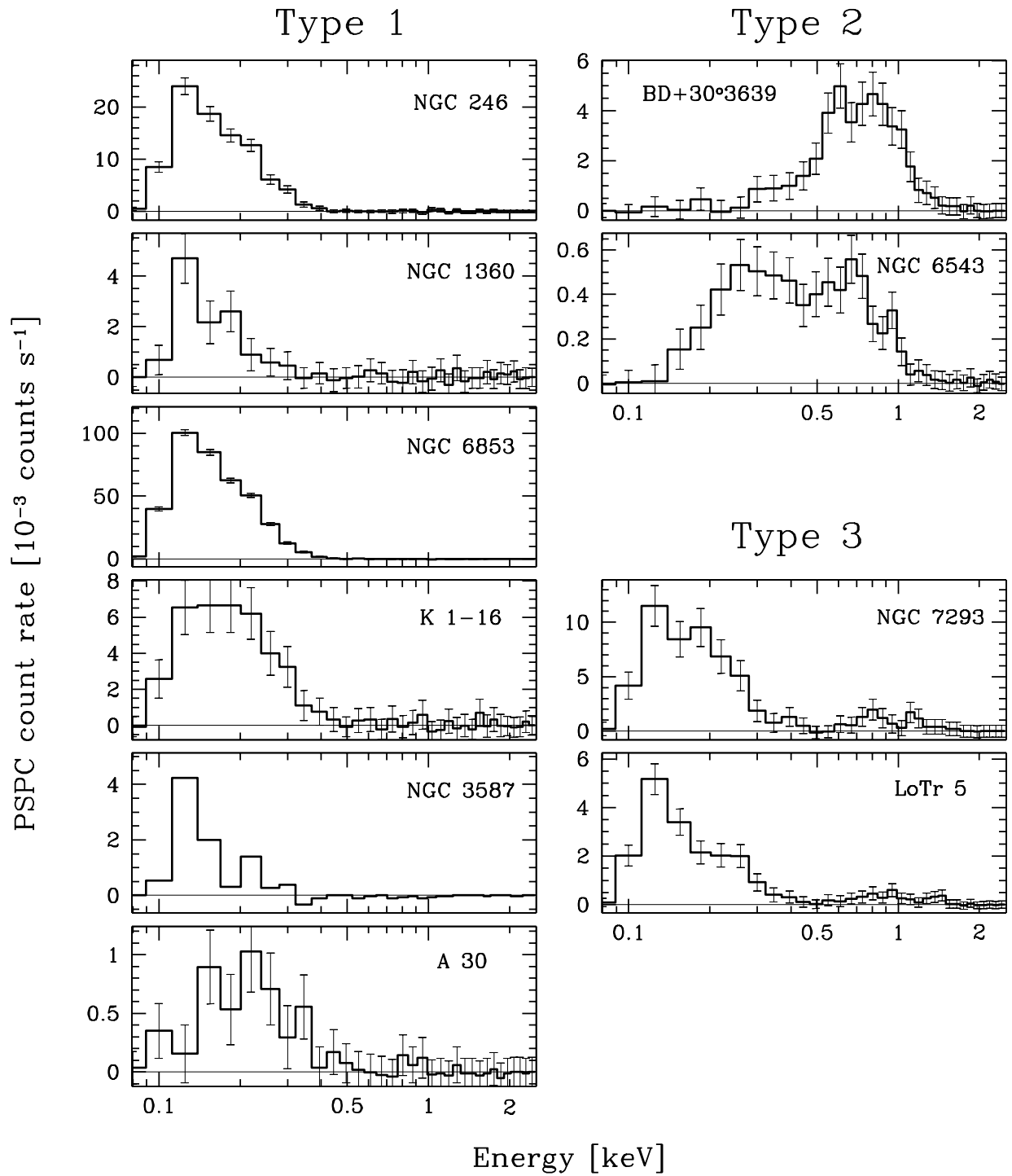


FIG. 3— X-ray spectra for the 10 PNs in the ROSAT PN sample with sufficient S/N to classify their spectral properties. The spectra clearly show that there are three distinct classes of X-ray emission observed in PNs.

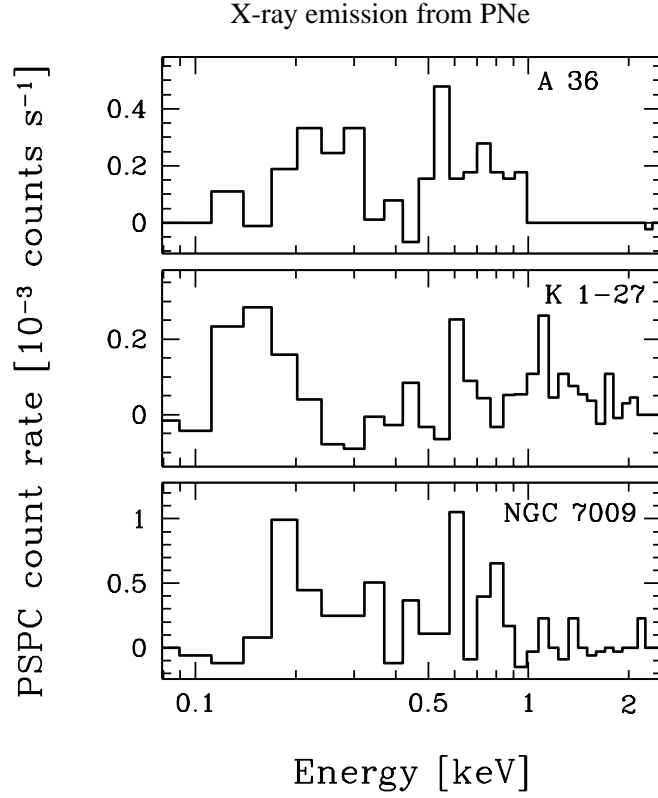


FIG. 4— X-ray spectra for the 3 PNs in the ROSAT PN sample with insufficient S/N to classify their spectral properties unambiguously. The lack of a prominent peak at 0.1–0.2 keV indicates that these spectra are most likely of Type 2.

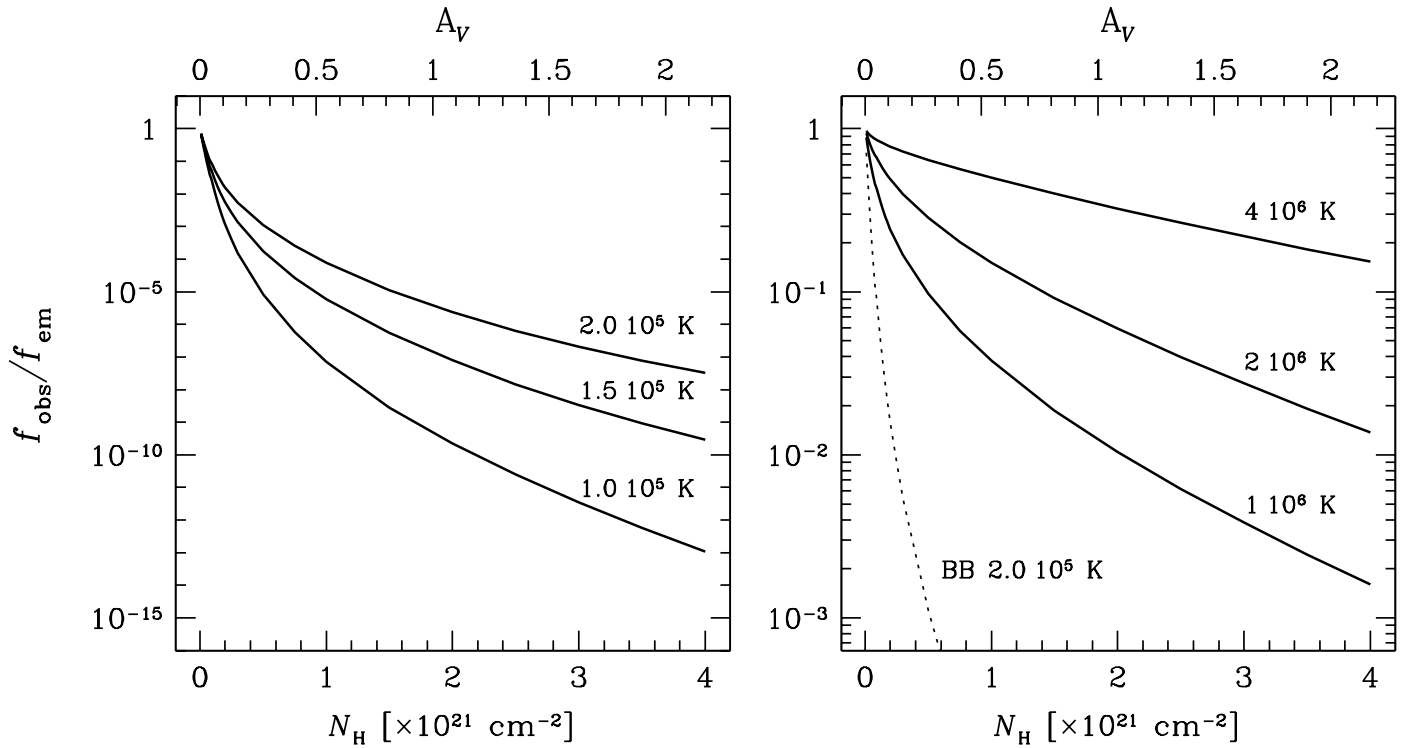


FIG. 5— Absorbed to unabsorbed flux ratio,  $f_{\text{abs}}/f_{\text{em}}$ , in the ROSAT PSPC band (0.1–2.4 keV) for a blackbody [*left panel*] and a thin plasma [*right panel*] emission model as a function of the absorption column density,  $N_H$  (or extinction  $A_V$ ). In order to better show the extreme difference in the detectability of emission from the two models, the curve corresponding to the highest temperature blackbody model ( $T_{\text{eff}} = 2.0 \times 10^5$  K) has also been included (*dotted line*) in the right panel.

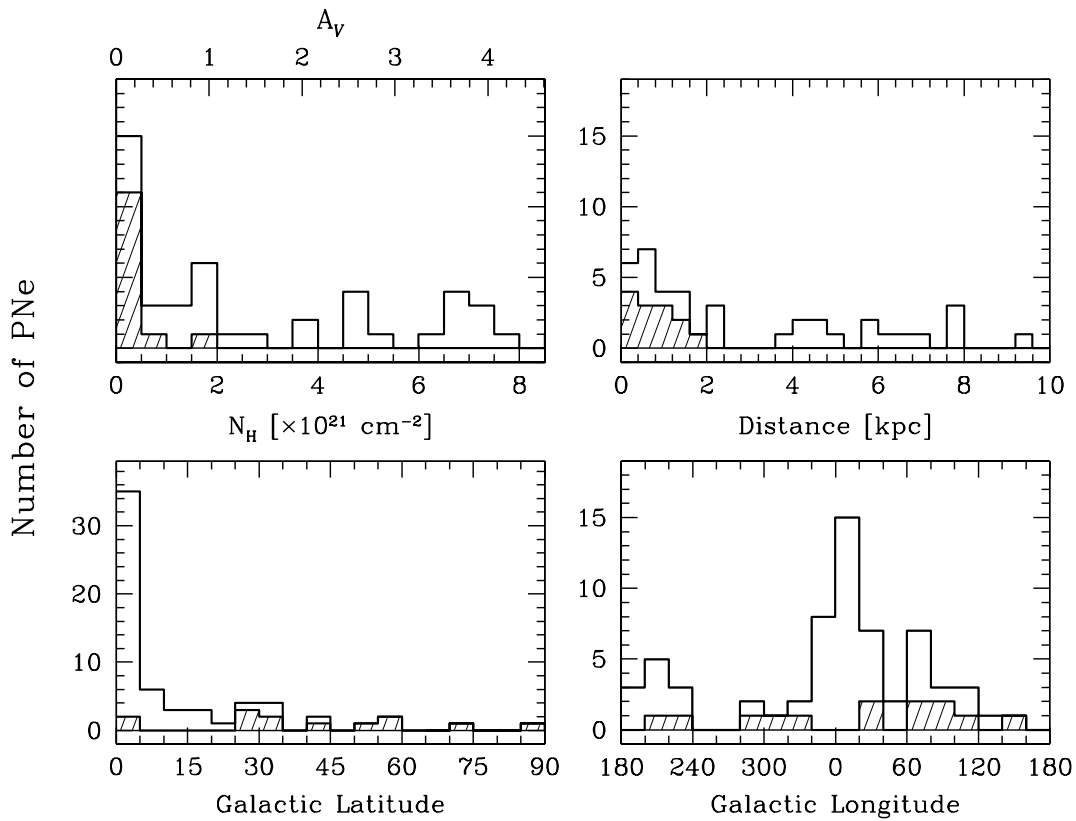


FIG. 6– Observed distributions of the galactic coordinates, column densities, and distances for the ROSAT PN sample. As in Figure 1, the shaded histogram shows the distribution of detected PNs while the open histogram shows the distribution of all PNs.

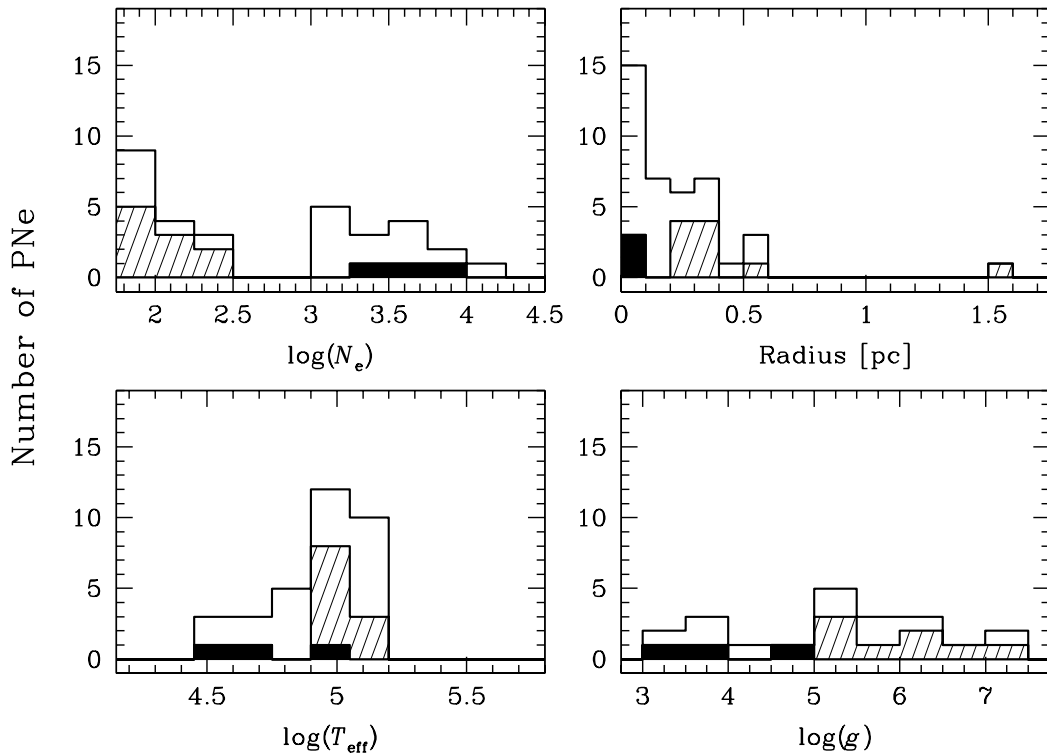


FIG. 7– Observed distributions of the effective temperature and gravity of the central stars, and nebular radius and density for the ROSAT PN sample (open histogram). The PNs with detected X-ray emission and Type 1 or 3 spectra are shown by the shaded histogram, whereas the PNs with Type 2 spectra are shown by the solid histogram.

This figure "fig2a.jpg" is available in "jpg" format from:

<http://arxiv.org/ps/astro-ph/0001404v1>

This figure "fig2b.jpg" is available in "jpg" format from:

<http://arxiv.org/ps/astro-ph/0001404v1>

This figure "fig2c.jpg" is available in "jpg" format from:

<http://arxiv.org/ps/astro-ph/0001404v1>



This figure "fig2d.jpg" is available in "jpg" format from:

<http://arxiv.org/ps/astro-ph/0001404v1>

This figure "fig2e.jpg" is available in "jpg" format from:

<http://arxiv.org/ps/astro-ph/0001404v1>